

Multi-UAV Trajectory Optimization for Bearing-Only Localization in GPS Denied Environments

Alfonso Sciacchitano^{*}, Liraz Mudrik[†], Sean Kragelund[‡], and Isaac Kaminer[§]
Naval Postgraduate School, Monterey, CA, 93943

Accurate localization of maritime targets by unmanned aerial vehicles (UAVs) remains challenging in GPS-denied environments. UAVs equipped with gimballed electro-optical sensors are typically used to localize targets, however, reliance on these sensors increases mechanical complexity, cost, and susceptibility to single-point failures, limiting scalability and robustness in multi-UAV operations. This work presents a new trajectory optimization framework that enables cooperative target localization using UAVs with fixed, non-gimballed cameras operating in coordination with a surface vessel. This estimation-aware optimization generates dynamically feasible trajectories that explicitly account for mission constraints, platform dynamics, and out-of-frame events. Estimation-aware trajectories outperform heuristic paths by reducing localization error by more than a factor of two, motivating their use in cooperative operations. Results further demonstrate that coordinated UAVs with fixed, non-gimballed cameras achieve localization accuracy that meets or exceeds that of single gimballed systems, while substantially lowering system complexity and cost, enabling scalability, and enhancing mission resilience.

^{*}Doctoral Student, Dept. of Mechanical and Aerospace Engineering, Email: alfonso.sciacchitano@nps.edu, Student Member AIAA.

[†]Postdoctoral Fellow, Dept. of Mechanical and Aerospace Engineering, Email: liraz.mudrik.ctr@nps.edu, Member AIAA.

[‡]Research Associate Professor, Dept. of Mechanical and Aerospace Engineering, Email: spkragel@nps.edu, Member AIAA.

[§]Professor, Dept. of Mechanical and Aerospace Engineering. Email: kaminer@nps.edu, Senior Member AIAA.

I. Introduction

Cooperative operations between unmanned aerial vehicles (UAVs) and unmanned surface vessels (USVs) enhance situational awareness, extend sensing range, and enable autonomous engagement in denied or contested environments [1]. Among these missions, target localization is mission-critical, demanding solutions that are accurate, robust, responsive, and cost-effective [2]. Traditional methods, such as global positioning system (GPS)-based tracking and active ranging (e.g., radar, LiDAR), perform well in permissive settings but degrade significantly under GPS-denied or electromagnetically contested conditions. Specifically, GPS can be jammed or spoofed, and active ranging sensors are both vulnerable to electronic countermeasures and risk revealing the platform's location through their own emissions. These limitations render them ill-suited for low-signature, long-endurance missions.

Passive alternatives, notably bearing-only measurements obtained from camera systems, address these challenges by using low-power electro-optical (EO) sensors to estimate target location through bearing measurements. Unlike active ranging systems, passive sensors do not emit signals, which reduces power consumption, lowers system cost, and enhances survivability by minimizing the risk of detection in contested environments. Additionally, many cooperative scenarios, such as UAV-assisted USV targeting of surface vessels, rely on relative geometry rather than absolute positioning, making passive sensing especially effective in denied environments [3].

Small fixed-wing UAVs equipped with passive EO sensors are well-suited for these applications. Their mechanically simple design and minimal power requirements contribute to a favorable size, weight, power, and cost (SWaP-C) profile, making them viable for endurance-limited, low-signature missions where stealth and agility are required, while also reducing cost, a critical factor given the high attrition rates expected in contested environments. The case for small fixed-wing UAVs is further underscored by recent operational losses of medium-altitude long-endurance platforms, such as the MQ-9 Reaper, with each exceeding \$30 million (USD) in unit cost [4]. Although these larger systems provide continuous target surveillance, their vulnerability in contested airspace significantly impacts overall mission success, as they are single points of failure. In contrast, coordinated low-cost

UAVs offer a resilient and economically sustainable alternatives for this mission type, as recent drone utilization has shown sortie costs of expendable low-altitude short range UAVs to be several thousand of dollars or less [5].

In this work, a group of UAVs estimate the positions of both an adversarial surface target and a collaborating USV using bearing-only measurements. With GPS unavailable, the USV cannot determine its own absolute position and instead relies on relative position estimates transmitted from the UAVs to establish the geometry needed for precision targeting.

As illustrated in Figure 1, each UAV acquires bearing-only measurements of both the adversarial target and the collaborating USV. These measurements are processed onboard the UAV to produce state estimates, which are then relayed to the collaborating USV at the conclusion of flight. Upon receiving these estimates, the USV fuses them into its master filter that determines the a posteriori estimate of the relative geometry, enabling precise targeting without using its own onboard sensors.

A. Operational and Dynamic Constraints

Prior studies on optimal observer motion for localization [6–8] prioritized estimation performance but omitted operational limitations such as sensor field-of-view (FOV), mission-area boundaries, and stealth requirements. Among prior studies, only a limited number have incorporated practical mission constraints. For example, [6] considered a minimum-time constraint, and [9] introduced communication-distance limits. Consequently, these existing localization formulations lack the necessary fidelity to remain viable under realistic mission conditions.

Addressing this gap requires modeling EO sensor FOV restrictions which necessitate trajectory planning to optimize measurements while leveraging Bayesian estimation methods while the targets are out-of-frame, as described in [10, Chap. 12]. Additionally, trajectories must account for bank-to-turn (BTT) UAV dynamics, a characteristic of fixed-wing UAVs that rely on coordinated turns in which roll commands produce heading changes [11]. This coupling between roll and yaw limits the UAV’s maneuverability and constrains the achievable flight paths, especially for fixed field-of-view (FFOV) sensors that cannot pivot independently of the airframe. Consequently, the

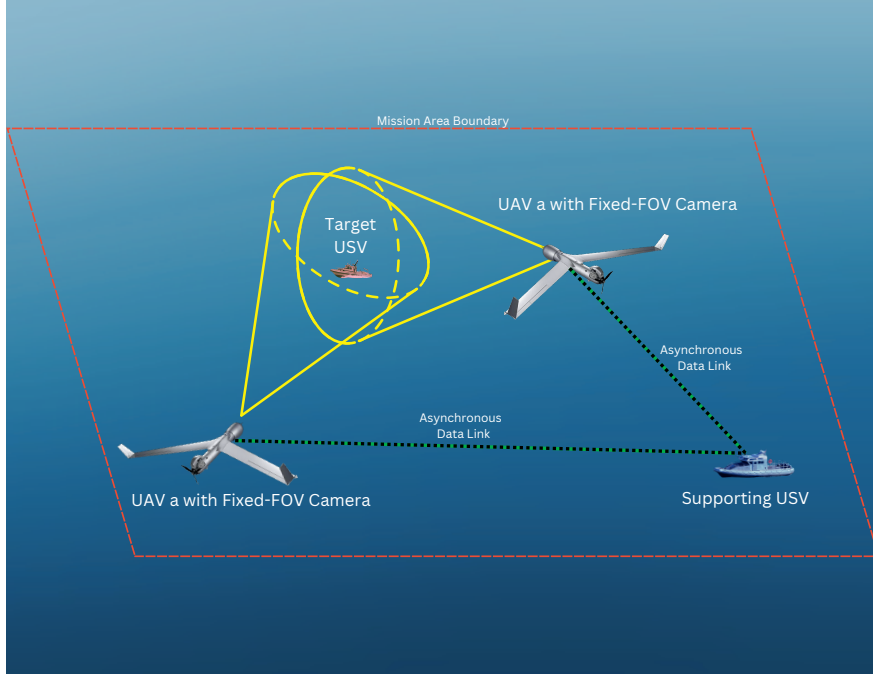


Fig. 1 Operational concept for cooperative localization in GPS-denied environments using fixed-wing UAVs with fixed-field-of-view cameras. Each UAV passively acquires bearing-only measurements of both the adversarial target USV and the collaborating USV using these onboard EO sensors. The measurements are processed locally to produce state estimates, which are transmitted asynchronously to the collaborating USV upon mission termination. The collaborating platform fuses the incoming estimates within a master filter, generating an a posteriori estimate of the relative geometry between itself and the target USV. This cooperative localization enables the collaborating USV to conduct precise targeting without onboard perception sensors or direct line-of-sight, while supporting decentralized operations within a bounded mission area.

optimization must explicitly consider BTT dynamics to ensure that planned trajectories remain dynamically feasible and that EO sensor line-of-sight (LOS) constraints are satisfied throughout the mission.

Additional constraints are imposed to maintain stealth and survivability, including no-fly zones (NFZs) around adversarial targets, bounded UAV-USV communication distances to minimize detection risk and energy usage, and adherence to operational airspace limits such as altitude ceilings and geographic boundaries [12]. By explicitly embedding these constraints, the present study extends existing localization frameworks to generate operationally realistic paths that enhance UAV survivability and maximize overall mission effectiveness.

B. Performance Metrics for Trajectory Optimization

A widely adopted metric for improving estimation performance is the Fisher information matrix (FIM), whose inverse yields the Cramér–Rao lower bound (CRLB), a fundamental lower bound on estimation error [10, 13]. In two-dimensional formulations, many researchers have chosen to maximize the determinant of the FIM to generate trajectories that yield information-rich measurements [6, 7, 14–16].

In three-dimensional target localization, [8] demonstrated that minimizing the trace of the CRLB is more robust and computationally stable than maximizing the determinant of the FIM. Specifically, they showed that minimizing the trace lead to faster convergence, higher optimization stability, and reduced sensitivity to local minima. These attributes are particularly valuable in trajectory optimization for bearing-only localization, where measurements are strongly influenced by sensor geometry and platform constraints. Conceptually, the trace of the CRLB is analogous to position dilution of precision (PDOP) in GPS, where lower PDOP values indicate more favorable satellite–receiver geometry and thus higher positioning accuracy. Similarly, minimizing the trace of the CRLB ensures better estimator performance by favoring trajectories that produce bearing measurements with higher information in constrained, three-dimensional environments. Despite these benefits, few studies have extended these principles to localization problems with practical considerations such as sensor constraints, mission bounds, and vehicle dynamics.

In this work, the performance index follows the formulation of [8] by adopting the trace of the posterior Cramér–Rao lower bound (PCRLB). The PCRLB, introduced by Van Trees *et al.*, provides a Bayesian lower bound on the estimator’s error covariance by incorporating prior uncertainty, information gained from new measurements, and process noise [13]. In the Gaussian case, the PCRLB defines an uncertainty ellipsoid around the estimated state, with the trace representing the sum of the variances along each principal axis, corresponding to the squared lengths of its semi-axes. Minimizing the trace of the PCRLB over the planning horizon guides the UAV along trajectories that not only enhance measurement geometry, but also effectively reduce overall uncertainty given the prior knowledge.

C. Numerical Optimization for Trajectory Design

Due to the inherent nonlinearities and complex constraints in information-driven trajectory design, closed-form analytical solutions are generally intractable. Consequently, this work employs direct numerical optimization techniques that convert the infinite-dimensional optimal control problem into a finite-dimensional nonlinear programming (NLP) formulation, enabling the generation of dynamically feasible trajectories under realistic sensing, kinematic, and environmental constraints.

Although Pseudospectral (PS) techniques are commonly employed due to their fast convergence and high accuracy [17], the fundamental limitation of PS methods is their non-uniform time discretization, which concentrates collocation points near the trajectory endpoints. Recent studies have demonstrated the utility of Bernstein polynomial basis functions over PS methods [18, 19], as they offer several favorable advantages such as uniform time discretization and avoidance of the Runge phenomenon [20]. Although they converge more slowly than PS methods, these advantages alone make them an effective choice for use in trajectory generation where smooth state and control profiles are essential.

D. Research Contributions

This study advances estimation-aware trajectory optimization for bearing-only localization by incorporating mission constraints, dynamic, and sensing constraints within a time-efficient optimization scheme. The formulation explicitly embeds FOV limits, BTT dynamics, NFZs, and communication boundaries, enabling dynamically feasible and operationally compliant trajectories usable by low-SWaP-C UAVs.

The conference version of this work focused on a single UAV [21], whereas this paper extends the work to coordinated multi-UAV operations in three dimensions and demonstrates that optimized trajectories yield substantial improvements in estimator performance relative to heuristic paths. The optimization results show that minimizing the trace of the PCRLB yields more informative motion geometries and substantially reduces localization error in Monte Carlo validation.

The analysis further quantifies how EO sensor selection, specifically cameras measuring visible

light, influences achievable estimation accuracy. In particular, the results identify the minimum number of FFOV UAVs with low-SWaP-C required to match or exceed the localization performance of a single UAV equipped with a gimballed camera.

E. Paper Organization

The remainder of the paper is organized as follows. Section II introduces the platform dynamics and sensor models, and formulates the joint trajectory optimization and estimation problem, incorporating key performance metrics derived from estimation theory. Section III then details two illustrative case studies. The first evaluates optimized trajectories versus heuristic solutions for a single FFOV UAV, while the second compares the performance and SWaP-C tradeoffs of a single UAV equipped with gimballed sensor a a coordinated team of FFOV UAVs. Finally, Section IV summarizes the research findings and highlights broader system-level insights derived from the study.

II. Problem Formulation

The trajectory optimization problem is defined for bearing-only localization using UAVs equipped with both gimballed and FFOV sensors. In a GPS-denied setting, the collaborating USV depends exclusively on the azimuth and elevation measurements from the UAVs to localize itself relative to the adversarial target. The objective is to design UAV flight paths that maximize localization accuracy by minimizing the trace of the PCRLB.

A. Platform Kinematics

Considering N UAVs, each is initialized to operate at a low, constant altitude for the duration of the mission. This altitude constraint serves three key operational purposes: (1) it minimizes the risk of detection by adversarial sensors and weapon systems, (2) it reduces the potential for fratricide when operating in proximity to other UAVs, and (3) it enables a simplified dynamic model by eliminating vertical state dynamics. While three-dimensional localization is performed using azimuth and elevation information derived from bearing-only measurements [22], the fixed-altitude assumption

justifies a reduction in the order of the UAV dynamics model. By constraining altitude, the vertical degree of freedom is removed, resulting in a planar (two-dimensional) dynamics formulation. This reduced-order model remains valid for surface-target engagement scenarios, where the elevation of stationary targets is effectively constant and does not influence maneuvering requirements.

To model the motion of UAV platforms, a BTT configuration is adopted. The continuous-time equations of motion for the UAV under this configuration are

$$\dot{x}_A(t) = V_A \cos \psi_A(t), \quad (1a)$$

$$\dot{y}_A(t) = V_A \sin \psi_A(t), \quad (1b)$$

$$\dot{z}_A(t) = 0, \quad (1c)$$

$$\dot{\psi}_A(t) = \frac{g}{V_A} \tan \phi_A(t), \quad (1d)$$

where $x_A(t)$, $y_A(t)$, and $z_A(t)$ represent the UAV's position in the inertial reference frame, V_A is the constant airspeed, and $\psi_A(t)$ is the heading angle. The roll angle $\phi_A(t)$ serves as the control input that commands the turn rate $\dot{\psi}_A(t)$, which is governed by gravitational acceleration g and the instantaneous roll command. Since excessive banking can lead to structural fatigue or instability, the roll angle is constrained by platform-specific limits

$$\phi^{\min} \leq \phi_A(t) \leq \phi^{\max}, \quad \forall t \in [0, t_f], \quad (2)$$

where ϕ^{\min} and ϕ^{\max} define the minimum and maximum allowable roll angles based on airframe design and maximum load factor. For each UAV, indexed by i , where $i = 1 \dots N$ the state and control vectors for the platform are defined as

$$\mathbf{x}_{A,i}(t) \triangleq \begin{bmatrix} x_{A,i}(t) & y_{A,i}(t) & z_{A,i}(t) & \psi_{A,i}(t) \end{bmatrix}^\top, \quad (3a)$$

$$\mathbf{u}_{A,i}(t) \triangleq \phi_{A,i}(t), \quad (3b)$$

where the control input consists solely of the roll angle. This formulation applies identically to

UAVs with both gimballed and body-fixed cameras.

For the UAV equipped with a gimballed camera, additional degrees of freedom are introduced by enabling independent camera articulation in azimuth and elevation, denoted as ψ_g and θ_g , respectively. This decouples the sensor pointing direction from the vehicle's heading, providing enhanced flexibility for target tracking. The problem formulation begins with a single UAV equipped with a gimballed camera, omitting the UAV index (subscript i) for notational clarity. Variables associated with the airframe are differentiated from variables associated with the camera gimbal by the subscripts A and g , respectively, producing the extended state and control vectors

$$\mathbf{x}_{A,g}(t) \triangleq \begin{bmatrix} x_A(t) & y_A(t) & z_A(t) & \psi_A(t) & \psi_g(t) & \theta_g(t) \end{bmatrix}^\top, \quad (4a)$$

$$\mathbf{u}_{A,g}(t) \triangleq \begin{bmatrix} \phi_A(t) & u_{\psi_g}(t) & u_{\theta_g}(t) \end{bmatrix}^\top, \quad (4b)$$

where the gimbal angles are governed by single integrator dynamics

$$\dot{\psi}_g(t) = u_{\psi_g}(t), \quad (5)$$

$$\dot{\theta}_g(t) = u_{\theta_g}(t). \quad (6)$$

The camera gimbal is constrained by angular rate limits to model the gimbal motor's actuators

$$u_{\psi_g}^{\min} \leq u_{\psi_g}(t) \leq u_{\psi_g}^{\max}, \quad \forall t \in [0, t_f], \quad (7)$$

$$u_{\theta_g}^{\min} \leq u_{\theta_g}(t) \leq u_{\theta_g}^{\max}, \quad \forall t \in [0, t_f]. \quad (8)$$

Figure 2 illustrates the coordinate conventions for the gimballed camera frame from both top-down and side perspectives. The UAV body-fixed frame is shown in blue and follows the standard aerospace convention with axes (x, y, z) pointing forward, right, and downward, respectively. The

gimbal frame, depicted in green, introduces two additional rotational degrees of freedom. These are azimuth ψ_g , defined as rotation about the UAV's vertical z-axis, and elevation θ_g , defined as rotation about the gimbal's local pitch axis. The Earth-fixed North-East-Down (NED) frame is shown in black for spatial reference.

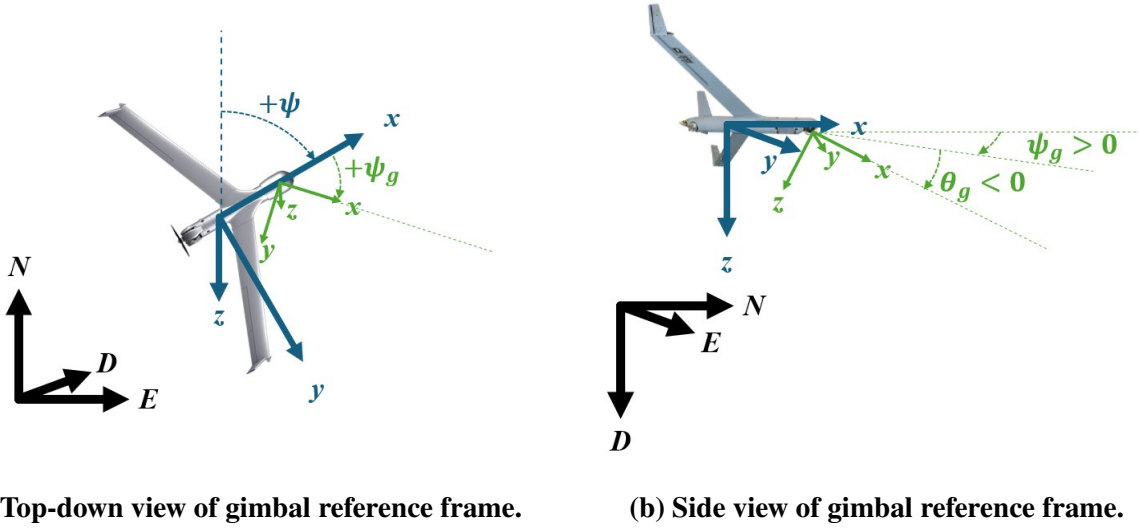


Fig. 2 Reference frame depiction for a strap-down gimballed camera system relative to the UAV.

B. Operational Constraints

To ensure effective target localization while preserving stealth, communication reliability, and overall mission feasibility, several operational constraints are imposed on UAV trajectories based on practical considerations such as minimizing the risk of counter-detection, enabling communications with the collaborating USV, and ensuring valid sensor-target geometry. Specifically, three primary classes of constraints are considered: (1) no-fly zone enforcement around the adversarial target, (2) bounded communication range with the collaborating platform, and (3) overall mission area limits imposed by operational boundaries.

1. No-Fly Zone Around the Target

To reduce the likelihood of counter-detection by adversarial systems, an NFZ is defined around the target of interest. UAV operations are constrained to remain outside this zone to avoid detection, classification, or engagement by the target's systems. The radius of the NFZ is selected based on the target's detection capabilities, the UAV's stealth profile, and environmental risk factors. The position vectors, $\mathbf{p}_{A,i}$, for each UAV indexed by i , are

$$\mathbf{p}_{A,i}(t) = \begin{bmatrix} x_{A,i}(t) & y_{A,i}(t) & z_{A,i}(t) \end{bmatrix}^\top \quad (9)$$

The position of the target USV, \mathbf{p}_T , is

$$\mathbf{p}_T(t) = \begin{bmatrix} x_T(t) & y_T(t) & z_T(t) \end{bmatrix}^\top. \quad (10)$$

Let r_{NFZ} denote the radius of the NFZ. The constraint is imposed as

$$\|\mathbf{p}_T(t) - \mathbf{p}_{A,i}(t)\| \geq r_{\text{NFZ}}, \quad \forall t \in [0, t_f] \quad (11)$$

where $\|\cdot\|$ denotes the Euclidean norm. This geometric exclusion ensures that UAVs remain outside the target's effective detection range throughout the mission timeline.

2. Maximum Communication Range

The UAVs must establish a communication link with the collaborating USV to exchange critical targeting data upon the completion of target localization. To maintain effective communication while ensuring security, a boundary condition is imposed on the maximum communication range at the terminal time, t_f . This constraint ensures that collected data can be transmitted effectively to the cooperative platform without risking counter-detection by external threats or increasing individual platform SWaP-C by requiring high-power communication systems for transmission.

Let r_{com} denote the maximum allowable communication range, and let

$$\mathbf{p}_{\text{USV}}(t) = \begin{bmatrix} x_{\text{USV}}(t) & y_{\text{USV}}(t) & z_{\text{USV}}(t) \end{bmatrix}^{\top} \quad (12)$$

be the position of the collaborating USV. The constraint is expressed as

$$\|\mathbf{p}_{\text{USV}}(t_f) - \mathbf{p}_{A,i}(t_f)\| \leq r_{\text{com}} \quad (13)$$

This communication boundary plays a critical role in preserving the functional integrity of the coordination strategy by enforcing a maximum boundary in which electromagnetic emissions are allowed.

3. Mission Area Bounds

In addition to local constraints near the target and collaborating USV, the UAV must operate within a bounded mission area that reflects the limits of available airspace, sensor coverage, and operational risk tolerance. These bounds are not imposed based on globally persistent knowledge or absolute geolocation, but are derived from prior mission planning, relative sensor constraints, and mission-relevant regions of interest.

Let the mission area be defined by a rectangular region aligned with the inertial coordinate axes. The admissible operating domain for each UAV, i , is bounded by

$$x_{\min} \leq x_{A,i}(t) \leq x_{\max}, \quad \forall t \in [0, t_f] \quad (14)$$

$$y_{\min} \leq y_{A,i}(t) \leq y_{\max}, \quad \forall t \in [0, t_f] \quad (15)$$

where x_{\min} , x_{\max} , y_{\min} , and y_{\max} , define the spatial extents of the mission area in the horizontal plane. Enforcing these bounds constrains UAV motion to mission-relevant regions, improves numerical conditioning of the optimization by avoiding infeasible or unbounded trajectories, and enables local enforcement using onboard sensors or cooperative data sharing. Collectively, the NFZ, communication range, and mission area bounds define the spatial limits wherein each UAV must

operate. These constraints are explicitly incorporated into the trajectory optimization formulation to ensure all generated trajectories remain feasible and mission compliant.

C. Sensor Modeling

Accurate modeling of the UAV’s onboard camera sensor is essential for enabling realistic trajectory optimization with bearing only measurements. The information gained from sensor measurements depends on the relative geometry between the UAV and the target(s), as well as sensor FOV constraints, which determine whether a given measurement is valid and how effectively it contributes to reducing target localization error. Here, information refers to the degree to which a measurement constrains the estimated position of the target, based on sensor-target geometry.

This section details the coordinate transformations required to compute relative measurements in the sensor frame, models the FOV constraint using smooth sigmoid-based functions to ensure compatibility with gradient-based optimization, and incorporates the augmented dynamic model needed for a UAV equipped with a gimballed camera. While the physical FOV is defined by strict angular limits, these are approximated using differentiable sigmoid functions to enable efficient numerical optimization [23]. The approximation captures the essential geometric constraints of the actual sensor model while avoiding the discontinuities associated with hard-threshold FOV enforcement.

1. Relative Position and Frame Transforms

Let ${}^I\mathbf{p}_{c,i}(t) \triangleq [x_{A,i}(t), y_{A,i}(t), z_{A,i}(t)]^\top$ represent the camera position in a local tangent (NED) frame for UAV i , assuming the camera is collocated with the UAV’s center of mass. The position of the target or collaborating USV, indexed via j , in the inertial frame is denoted ${}^I\mathbf{p}_j(t) \triangleq [x_j(t), y_j(t), z_j(t)]^\top$. Position relative to the UAV is

$${}^I\Delta\mathbf{p}_{i,j}(t) \triangleq {}^I\mathbf{p}_j(t) - {}^I\mathbf{p}_{c,i}(t). \quad (16)$$

Position with respect to the UAV’s body-fixed camera frame is

$${}^c \mathbf{p}_{i,j}(t) = \mathbf{R}_I^{c,i}(t) {}^I \Delta \mathbf{p}_{i,j}(t) \quad (17)$$

where $\mathbf{R}_I^{c,i}(t)$ denotes the rotation matrix from the inertial to the camera frame of UAV i , constructed from sequential rotations by the yaw, pitch, and roll angles, respectively

$$\mathbf{R}_I^{c,i}(t) = \mathbf{R}(\phi_i(t)) \mathbf{R}(\theta_i(t)) \mathbf{R}(\psi_i(t)). \quad (18)$$

For a single UAV equipped with a gimballed camera, we can omit the subscript i and express this relative position in the gimbal frame with two additional rotations by the commanded azimuth ψ_g and elevation θ_g angles

$${}^c_g \mathbf{p}_j(t) = R_c^{c_g}(t) {}^c \mathbf{p}_j(t), \quad (19)$$

where

$$\mathbf{R}_c^{c_g}(t) = \mathbf{R}(\theta_g(t)) \mathbf{R}(\psi_g(t)). \quad (20)$$

For either camera type, the sensor extracts azimuth (α_j) and elevation (β_j) bearing angles as

$$\alpha_{i,j}(t) \triangleq \text{atan2} \left({}^c_i r_{y,i,j}(t), {}^c_i r_{x,i,j}(t) \right), \quad (21a)$$

$$\beta_{i,j}(t) \triangleq \tan^{-1} \frac{{}^c_i r_{z,i,j}(t)}{\sqrt{({}^c_i r_{x,i,j}(t))^2 + ({}^c_i r_{y,i,j}(t))^2}}. \quad (21b)$$

2. FOV Constraints

Each camera has a limited FOV defined by azimuth and elevation bounds. The target and the collaborating USV, indexed by j , are considered visible to UAV i if their camera-frame azimuth and elevation angles satisfy the following angular FOV constraints

$$\alpha_{\min} \leq \alpha_{i,j}(t) \leq \alpha_{\max}, \quad \beta_{\min} \leq \beta_{i,j}(t) \leq \beta_{\max}. \quad (22)$$

When either angle exceeds these limits, an out-of-frame event occurs, meaning the target temporarily leaves the sensor's FOV. These events interrupt the acquisition bearing measurements and reduce information gain. To account for this effect in the optimization, visibility is modeled as a continuous weighting function that smoothly decreases to zero as the target approaches the FOV boundary. This allows the optimizer to anticipate and minimize information loss due to these out-of-frame conditions.

To enable gradient-based optimization over real-valued decision variables, each angular visibility constraint in Eq. (22) is approximated using a smooth, parameterized sigmoid function. This produces a continuously differentiable surrogate for the original discontinuous indicator function, which outputs values in $[0, 1]$ and approximates binary visibility decisions in a differentiable manner. The sigmoid function for each angular constraint is

$$\mathbb{I}_{\delta_{\text{limit}}} = \frac{1}{1 + e^{k(\delta - \delta_{\text{limit}})}}, \quad (23)$$

where δ is the measured angle, δ_{limit} is the threshold, and $k > 0$ controls the steepness of the transition.

The complete approximation of the FOV indicator function, denoted $\mathbb{I}_{FOV_{i,j}}(t)$, is then constructed as the product of four sigmoid-based functions that correspond to the upper and lower bounds on the azimuth and elevation angles in the sensor FOV,

$$\mathbb{I}_{FOV_{i,j}}(t) = \mathbb{I}_{\alpha_{\min,i,j}}(t) \cdot \mathbb{I}_{\alpha_{\max,i,j}}(t) \cdot \mathbb{I}_{\beta_{\min,i,j}}(t) \cdot \mathbb{I}_{\beta_{\max,i,j}}(t), \quad (24)$$

where each term smoothly enforces one side of the angular visibility, ensuring that $\mathbb{I}_{FOV_{i,j}}(t) \in [0, 1]$. Fig. 3 illustrates how overlapping sigmoid functions approximate the angular visibility bounds for azimuth angles $\alpha \in [-\frac{\pi}{4}, \frac{\pi}{4}]$.

The resulting visibility function $\mathbb{I}_{FOV_{i,j}}(t)$, provides a continuous and differentiable approximation of target visibility. This property preserves the smoothness required for use with gradient-enabled numerical solvers [24], and ensures that information weighting remains physically meaningful

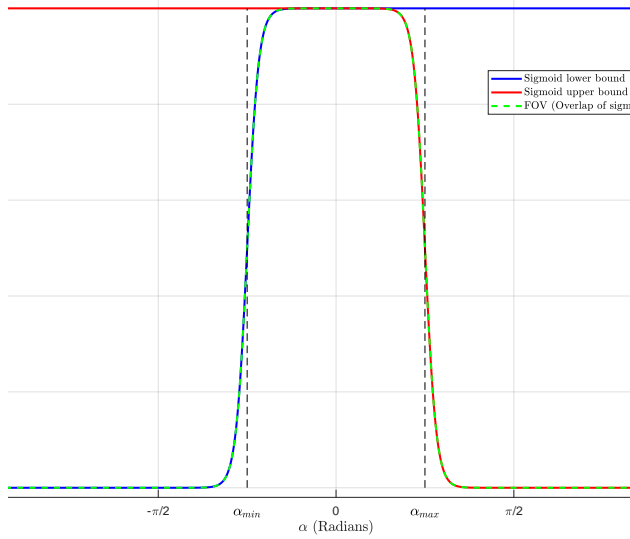


Fig. 3 Smooth approximation of FOV constraints using overlapping sigmoid functions.

during out-of-frame transitions.

D. Performance Index – The PCRLB

To quantify the estimation performance of a candidate UAV trajectory, the PCRLB is adopted as the primary performance index. The PCRLB provides a theoretical lower bound on the covariance of any Bayesian estimator and serves as a proxy for assessing localization accuracy in the bearing-only tracking scenarios considered.

The inclusion of the prior is critical in this work because both the target and the collaborating USV are assumed stationary. The prior represents the initial covariance of the state estimate before any bearing measurements are obtained, reflecting the uncertainty associated with pre-mission cueing or previous sensing. In practice, this prior may originate from external intelligence or surveillance assets such as radar, satellite imagery, or surface-based sensors that provide coarse initial localization of the target and collaborating USV. As new measurements are collected, this

prior information is updated through the estimation process, yielding a posterior bound that reflects the cumulative information gained.

The trace of this matrix, which sums the variances along each state dimension, serves as a scalar measure of total position estimation uncertainty. This scalar quantity is conceptually analogous to the PDOP used in GPS-based systems, where PDOP quantifies how the geometric configuration of satellites amplifies the impact of measurement noise on position accuracy. Similarly, minimizing the trace of the PCRLB favors trajectories that improve sensing geometry and reduce the theoretical lower bound on estimation error, thereby enhancing overall localization performance.

EO sensors in general operate at fixed sampling frequencies, therefore, this work adopts a discrete-time approach for modeling bearing measurements. This formulation aligns naturally with how sensor data is generated and processed onboard the UAV, as measurements arrive at regular intervals determined by hardware and computational constraints. Under these conditions, the information relevant to estimation performance also accumulates discretely in time, making the discrete formulation of the FIM and PCRLB both practical and consistent with standard filtering and numerical optimization methods.

The recursive form of the PCRLB used in this work follows the formulation of [25], where the prior information is propagated through the FIM to account for both prediction and measurement updates. For the stationary target case considered here, the recursion simplifies to a sequential accumulation of bearing measurement information, starting from the initial covariance corresponding to the prior uncertainty. This ensures that the resulting bound reflects both the initial knowledge of the target state and the incremental information gained from new measurements. The posterior bound satisfies

$$\mathbb{E}\{[\hat{\mathbf{x}}_{k|k} - \mathbf{x}_k][\hat{\mathbf{x}}_{k|k} - \mathbf{x}_k]^\top\} \geq \mathbf{PCRLB}(k) = \mathbf{FIM}(k)^{-1}, \quad (25)$$

where $\hat{\mathbf{x}}_{k|k}$ is the estimated target state and \mathbf{x}_k is the true state at time k .

The FIM for a stationary target j , observed by UAV i over N_k discrete time steps, is computed according to standard formulations in estimation theory [10, 13] as

$$\mathbf{FIM}_j = \sum_{k=1}^{N_k} \left(\frac{\partial \mathbf{h}_{i,j}(\mathbf{x}_i(k), \mathbf{x}_j(k))}{\partial \mathbf{x}_j(k)} \right)^\top \mathbf{R}_{i,j}^{-1}(k) \left(\frac{\partial \mathbf{h}_{i,j}(\mathbf{x}_i(k), \mathbf{x}_j(k))}{\partial \mathbf{x}_j(k)} \right), \quad (26)$$

where $\mathbf{h}_{i,j}(\mathbf{x}_i(k), \mathbf{x}_j(k)) = [\alpha_{i,j}(k), \beta_{i,j}(k)]^\top$ contains the azimuth and elevation angles from UAV i to target j and $\mathbf{R}_{i,j}(k)$ is the corresponding measurement noise covariance matrix

$$\mathbf{R}_{i,j}(k) = \begin{bmatrix} \sigma_{\alpha_{i,j}}^2(k) & 0 \\ 0 & \sigma_{\beta_{i,j}}^2(k) \end{bmatrix}. \quad (27)$$

The measurement functions for azimuth and elevation are defined in a NED coordinate frame by the geometric relations

$$\mathbf{h}_{i,j}(\mathbf{x}_i(k), \mathbf{x}_j(k)) \triangleq \begin{bmatrix} \alpha_{i,j} \\ \beta_{i,j} \end{bmatrix}, \quad (28)$$

where $\mathbf{x}_i(k)$ are the known positions of UAV i , assumed to be available from prior information such as third-party targeting or mission planning data and maintained via onboard inertial measurements, and $\mathbf{x}_j(k)$ are the unknown target states to be estimated.

The Jacobian of the measurement function $\mathbf{h}_{i,j}(\mathbf{x}_i(k), \mathbf{x}_j(k))$ with respect to the target state $\mathbf{x}_j(k)$ is adapted from [8] and is given by

$$\frac{\partial \mathbf{h}_{i,j}(\mathbf{x}_i(k), \mathbf{x}_j(k))}{\partial \mathbf{x}_j(k)} = \begin{bmatrix} \frac{\partial \alpha_{i,j}}{\partial x_j} & \frac{\partial \alpha_{i,j}}{\partial y_j} \\ \frac{\partial \beta_{i,j}}{\partial x_j} & \frac{\partial \beta_{i,j}}{\partial y_j} \end{bmatrix}_k = \begin{bmatrix} -\frac{r_{y,i,j}}{r_{x,i,j}^2 + r_{y,i,j}^2} & \frac{r_{x,i,j}}{r_{x,i,j}^2 + r_{y,i,j}^2} \\ -\frac{r_{x,i,j}r_{z,i,j}}{r_{i,j}^2 \sqrt{r_{x,i,j}^2 + r_{y,i,j}^2}} & -\frac{r_{y,i,j}r_{z,i,j}}{r_{i,j}^2 \sqrt{r_{x,i,j}^2 + r_{y,i,j}^2}} \end{bmatrix}_k, \quad (29)$$

where $r_{i,j}$ is the euclidean distance between UAV i and target j . Note that although the target and UAV positions include a z-component, changes in the vertical direction are not estimated. Since the UAV and target altitudes are assumed to be known and constant, the measurement Jacobian is reduced to a 2×2 form involving only the x and y components of the target state.

To reflect realistic sensing constraints, each FIM contribution is weighted by the continuous

visibility factor $\mathbb{I}_{FOV_{i,j}}(k)$ defined in Eq. (24). Additionally, external cuing is incorporated in the initialization of the FIM where the initial prior enters the information matrix as $\mathbf{P}_{0,j}^{-1}$. This prior is distributed across all UAVs using a uniform weighing rule

$$\lambda_i = \frac{1}{N_{\text{UAV}}}, \quad \sum_{i=1}^{N_{\text{UAV}}} \lambda_i = 1, \quad (30)$$

where λ_i are the uniform weights that sum to one. The fused formulation accounting for the combined information gain by all UAVs is given by

$$\mathbf{FIM}_j = \sum_{i=1}^{N_{\text{UAV}}} \left\{ \lambda_i \mathbf{P}_{0,j}^{-1} + \sum_{k=1}^{N_k} \mathbb{I}_{FOV_{i,j}}(k) \left(\frac{\partial \mathbf{h}_{i,j}(\mathbf{x}_i(k), \mathbf{x}_j(k))}{\partial \mathbf{x}_j(k)} \right)^T \mathbf{R}_{i,j}^{-1}(k) \left(\frac{\partial \mathbf{h}_{i,j}(\mathbf{x}_i(k), \mathbf{x}_j(k))}{\partial \mathbf{x}_j(k)} \right) \right\} \quad (31)$$

The resulting PCRLB, derived from the inverse of this FIM, represents a lower bound on the estimation error covariance for target j . Minimizing the trace of the PCRLB was found to be an effective performance index for optimization in [8]. Therefore, we utilize the trace of the PCRLB in this work to facilitate direct performance comparisons across different UAV configurations and mission scenarios.

E. Optimization

The trajectory design problem is formulated as a constrained optimization problem that minimizes a weighted objective function combining estimation performance and mission duration. This multi-objective formulation captures the trade-off between target localization performance and time efficiency, subject to the kinematic, sensing, and operational constraints introduced in prior sections.

The cost function incorporates the trace of the PCRLB for both the target, PCRLB_T , and the collaborating USV, $\text{PCRLB}_{\text{USV}}$. Tunable parameters, $w_1, w_2 \in [0, 1]$, are used to control their relative importance for localization, respectively. An additional penalty term scaled by $w_3 \geq 0$ is included to penalize unnecessarily long trajectories. The cost function formulation for N UAVs is

$$\min_{\mathbf{x}(t), \mathbf{u}(t)} J = w_1 \cdot \text{Tr}(\text{PCRLB}_T) + w_2 \cdot \text{Tr}(\text{PCRLB}_{\text{USV}}) + w_3 \cdot t_f, \quad (32)$$

where $\mathbf{x}(t)$ and $\mathbf{u}(t)$ denote the state and control trajectories for all UAVs, $\text{Tr}(\cdot)$ is the matrix trace operator, and t_f is the final time of the mission. This cost function is subject to the following constraints

$$\dot{\mathbf{x}}_i(t) = f(\mathbf{x}_i(t), \mathbf{u}_i(t)), \quad (33a)$$

$$\phi^{\min} \leq \phi_A(t) \leq \phi^{\max}, \quad \forall t \in [0, t_f], \quad (33b)$$

$$x_{\min} \leq x_{A,i}(t) \leq x_{\max}, \quad \forall t \in [0, t_f], \quad (33c)$$

$$y_{\min} \leq y_{A,i}(t) \leq y_{\max}, \quad \forall t \in [0, t_f], \quad (33d)$$

$$\|\mathbf{p}_T(t) - \mathbf{p}_{A,i}(t)\| \geq r_{\text{NFZ}}, \quad \forall t \in [0, t_f], \quad (33e)$$

$$\|\mathbf{p}_{\text{USV}}(t_f) - \mathbf{p}_{A,i}(t_f)\| \leq r_{\text{com}}. \quad (33f)$$

These constraints ensure that the resultant UAV trajectories are dynamically feasible and do not violate operational considerations. However, because the trajectory and control profiles are continuous functions of time, this formulation represents an infinite-dimensional optimization problem whose exact solution is generally intractable. This motivates the use of numerical approximation methods to obtain computationally feasible solutions.

F. Bernstein Approximation

To obtain a tractable formulation, the problem is transformed into a finite-dimensional NLP problem by approximating the continuous-time state and control trajectories for each UAV using Bernstein polynomials. This parameterization is particularly advantageous because the Bernstein basis is the only known polynomial basis that operates with uniformly spaced time nodes, ensuring compatibility with fixed sensor sampling rates and avoiding the Runge phenomenon observed in other polynomial approximations [20].

The Bernstein basis polynomial of degree n is defined as

$$b_{j,n}(t) = \binom{n}{j} \frac{t^j (t_f - t)^{n-j}}{t_f^n}, \quad j = 0, \dots, n, \quad \forall t \in [0, t_f] \quad (34)$$

where the binomial coefficient is

$$\binom{n}{j} = \frac{n!}{j!(n-j)!} \quad (35)$$

The corresponding time nodes are equidistant and given by

$$t_j = \frac{j}{n} t_f, \quad j = 0, \dots, n \quad (36)$$

where $t_f > 0$ is given. The state and control trajectories are then approximated as linear combinations of Bernstein basis functions

$$\mathbf{x}(t) \approx \sum_{j=0}^n \bar{\mathbf{x}}_{j,n} b_{j,n}(t), \quad (37)$$

$$\mathbf{u}(t) \approx \sum_{j=0}^n \bar{\mathbf{u}}_{j,n} b_{j,n}(t), \quad (38)$$

where $\bar{\mathbf{x}}_{j,n} \in \mathbb{R}^{n_x}$ and $\bar{\mathbf{u}}_{j,n} \in \mathbb{R}^{n_u}$ are the Bernstein coefficients for the states and controls, respectively.

These coefficients are used to define the matrices

$$\bar{\mathbf{x}}_n = \begin{bmatrix} \bar{\mathbf{x}}_{0,n} & \dots & \bar{\mathbf{x}}_{n,n} \end{bmatrix} \in \mathbb{R}^{n_x \times (n+1)}, \quad (39)$$

$$\bar{\mathbf{u}}_n = \begin{bmatrix} \bar{\mathbf{u}}_{0,n} & \dots & \bar{\mathbf{u}}_{n,n} \end{bmatrix} \in \mathbb{R}^{n_u \times (n+1)} \quad (40)$$

A key advantage of Bernstein polynomials is their well-defined differentiation property, which applies to any function approximated by the Bernstein basis

$$\dot{\mathbf{x}}_n(t) = \sum_{j=0}^{n-1} \frac{n}{t_f} (\bar{\mathbf{x}}_{j+1,n} - \bar{\mathbf{x}}_{j,n}) b_{j,n-1}(t) = \sum_{j=0}^{n-1} \sum_{i=0}^n \bar{\mathbf{x}}_{i,n} \mathbf{D}_{i,j} b_{j,n-1}(t) \quad (41)$$

where $\mathbf{D}_{i,j}$ is the (i, j) -th entry of the differentiation matrix as described in [19].

For a dynamic model satisfying $\dot{\mathbf{x}}_i(t) = f(\mathbf{x}_i(t), \mathbf{u}_i(t))$ and a number $1 > \delta > 0$, this differential constraint is approximated using a relaxation

$$\left\| \sum_{i=0}^n \bar{\mathbf{x}}_{i,n} \mathbf{D}_{i,j} - \mathbf{f}(\bar{\mathbf{x}}_{j,n}, \bar{\mathbf{u}}_{j,n}) \right\| \leq \delta^n, \quad \forall j = 0, \dots, n \quad (42)$$

where δ^n is a relaxation that converges to zero as $n \rightarrow \infty$. Another important property is that any Bernstein approximation lies within the convex hull of its control points

$$\min_{j=0, \dots, n} \bar{\mathbf{x}}_{j,n} \leq \mathbf{x}_n(t) \leq \max_{j=0, \dots, n} \bar{\mathbf{x}}_{j,n} \quad \forall t \in [0, t_f] \quad (43)$$

This property allows inequality constraints, such as the mission boundaries, to be enforced directly on the Bernstein control points, $\bar{\mathbf{x}}_{j,n}$. Since the trajectory cannot exceed the maximum values of these control points, enforcing constraints at the control points guarantees they are satisfied over the entire continuous trajectory, which simplifies constraint enforcement during the optimization process. For geometric constraints that define exclusion regions such as the NFZ, the convex-hull property provides an approximate guarantee. As long as the convex hull of the control points does not intersect the restricted region, the corresponding trajectory will also remain feasible.

Further detail on the use of Bernstein polynomials for trajectory generation problems are provided in [18–20, 26–29].

G. Federated Sensor Fusion via Extended Kalman Filtering

One architecture for multi-UAV target localization is a centralized approach in which the collaborating USV receives all bearing-only measurements from the UAVs and processes them within a single, global extended Kalman filter (EKF). While this method yields consistent and fully fused estimates, it requires the collaborating USV to maintain continuous, high-bandwidth communication with all UAVs throughout the mission, which incurs a higher SWaP-C burden.

To overcome this limitation, this work employs a federated Kalman filter (FKF) that conducts

data fusion at the conclusion of the mission. For coordinated target localization by multiple FFOV UAVs, each UAV independently tracks the target and collaborating USVs using a local EKF based on its own bearing measurements. These local EKFs run in parallel across the team of UAVs throughout the mission, producing time-varying state estimates $\mathbf{x}_{i,j}(k)$ and associated covariance matrices $\mathbf{P}_{i,j}(k)$ for each target j .

To synthesize these estimates into a single, system-level estimate, a FKF is applied at the final time step, after each UAV has completed its data collection and returned to the collaborating USV. This federated fusion step enables centralized aggregation of all local estimates using an information-weighted consensus rule. The FKF is computed according to standard estimation formulations [30–32] as

$$\mathbf{x}_j(k_f) = \left(\sum_{i=1}^{N_{\text{UAV}}} \mathbf{P}_{i,j}(k_f)^{-1} \right)^{-1} \sum_{i=1}^{N_{\text{UAV}}} \mathbf{P}_{i,j}(k_f)^{-1} \mathbf{x}_{i,j}(k_f), \quad (44)$$

$$\mathbf{P}_f(k_f) = \left(\sum_{i=1}^{N_{\text{UAV}}} \mathbf{P}_{i,j}(k_f)^{-1} \right)^{-1}, \quad (45)$$

where k_f denotes the final fusion time, and N_{UAV} is the number of participating UAVs. This formulation ensures consistent fusion without requiring inter-UAV communication or centralized processing during flight, making it compatible with bandwidth-limited systems such as those designed for low-SWaP-C.

The initialization of each local EKF is tied to the trajectory optimization process. Prior to deployment, each UAV is initialized with a common estimate of the target and USV states, derived from third-party cuing or prior mission knowledge. This shared prior defines the initial state and covariance used for estimator initialization. To prevent double counting during federated fusion, the initialization of the prior information is partitioned across UAVs as shown in Eq. (30). Importantly, this is the same covariance used to initialize the trajectory optimization, ensuring that planned trajectories are shaped to reduce uncertainty relative to the actual estimator initialization. As a result, both planning and estimation are aligned to maximize the value of each UAV’s individual

measurement given the expected state uncertainty at mission start.

By concentrating data fusion at the terminal step, this FKF-based approach enables robust, low-bandwidth cooperative localization without sacrificing estimator consistency. It supports scalable, federated architectures where FFOV UAVs can operate independently yet still contribute effectively to a shared targeting solution in GPS-denied or electromagnetically contested environments.

III. Results

Traditionally, UAV path planning for localization has relied on heuristic trajectories. These trajectories, such as the racetrack pattern or circular orbit, are easy to implement and are consistent with a legacy doctrine. While operationally convenient, these paths may fail to maximize information gain. In contrast, trajectories optimized with an information-theoretic objective such as minimizing the trace of the PCRLB, can significantly enhance localization accuracy and estimator performance. By explicitly accounting for time-varying geometry, visibility constraints, and sensor FOV limitations, these optimized paths are tailored to mission objectives, thereby enabling more intelligent and effective UAV operations.

Beyond performance metrics, trajectory optimization must be considered not only from the perspective of estimation performance but also within the broader context of system-level constraints. SWaP-C considerations, especially those tied to the airframe and sensor configuration, have a direct impact on platform design and operational deployment. Optimization may reduce flight time or the number of vehicles required, but platform-level design tradeoffs, such as the use of mechanically gimballed versus FFOV camera sensors, also play a pivotal role in determining system suitability. These tradeoffs enable trajectory optimization to emerge as both a control-theoretic enhancement and an enabler of more affordable and deployable system designs.

The interdependence of estimation accuracy, flight path design, and hardware configuration is highlighted in the case studies that follow. The first case study compares a heuristic racetrack trajectory with an optimized path for a single FFOV UAV, focusing on how trajectory shape alone influences localization performance.

The second case study evaluates the tradeoffs between a single UAV equipped with a gimballed camera and a coordinated team of FFOV UAVs. While the gimballed platform benefits from independent sensor articulation, it incurs a higher SWaP-C burden. The FFOV team, however, leverages multi-UAV coordination to match or exceed localization performance, demonstrating that distributed sensing systems can achieve high fidelity at reduced cost and greater redundancy.

Throughout the results, the scalar bound $\sqrt{\text{Tr}(\text{PCRLB})}$ is used to enable a direct, unit-consistent comparison with EKF and FKF Monte Carlo root mean square errors (RMSEs). The optimizer minimizes $\text{Tr}(\text{PCRLB})$, but all values, figures, and tables present $\sqrt{\text{Tr}(\text{PCRLB})}$. Key simulation constants and optimization parameters used in this study are summarized in IV.

Case Study 1: Racetrack vs Optimal FFOV UAV Trajectory After Retasking

This case study compares two different localization strategies for a single FFOV UAV following the unexpected discovery of a target during a broader maritime search mission as depicted in Fig. 4. The scenario models a common operational context in which UAVs conduct generic surveillance until cued by external assets, such as manned platforms or distributed sensors, to localize an identified target. Following localization, the UAV must enter within a designated communication range to report the target’s location relative to the collaborating USV.

At the moment of re-tasking, the UAV’s position is randomized within a bounded mission area to simulate the uncertainty inherent in real-world deployment. The importance of localizing both USVs and reducing mission time are equally important. From this initial state, two localization strategies are considered.

The first approach utilizes a heuristic trajectory, commonly referred to as a “racetrack” pattern. This trajectory consists of an ellipsoid-like flight path designed to remain outside of the designated NFZ while attempting to maintain continuous LOS to the target. Upon re-tasking, the UAV immediately enters the racetrack pattern to collect bearing-only measurements. While operationally straightforward, the racetrack approach is not designed to optimally localize a target while being time-efficient.

In contrast, the second approach employs Bernstein polynomial parameterization and numerical optimization to generate a feasible trajectory which minimizes the $\text{Tr}(\text{PCRLB})$ for this mission. The trajectory is computed offline and explicitly incorporates vehicle kinematics, sensor FOV constraints, and operational limits such as NFZ boundary and the communication constraint. The resulting path adjusts the UAV's geometry to maximize bearing angle rate and maintain information-rich relative positions. While non-intuitive, this trajectory strategically exploits the UAV's maneuverability to maximize information gain within the allowed sensing and operational constraints.

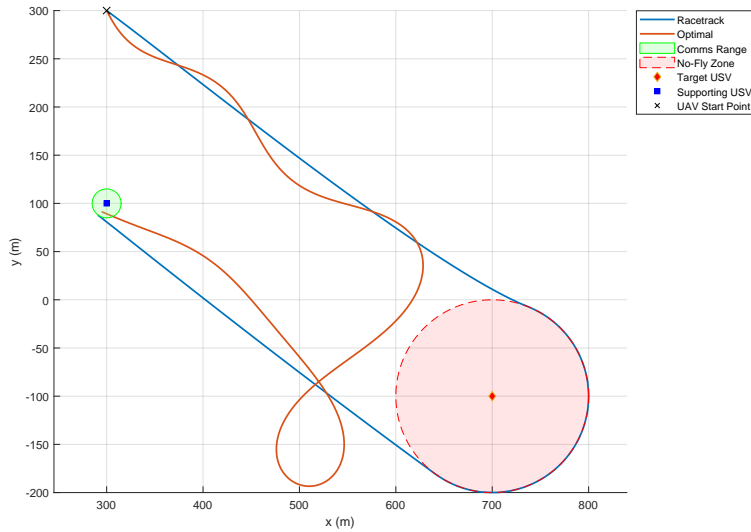


Fig. 4 Heuristic UAV racetrack trajectory vs optimized Bernstein trajectory.

Each trajectory is evaluated in terms of the $\text{Tr}(\text{PCRLB})$, which serves as the design metric. The EKF is then separately employed in Monte Carlo trials to assess whether practical estimation performance approaches this theoretical lower bound. It is important to emphasize that the trace of the PCRLB is used as the design and evaluation metric, representing the best achievable performance for an estimator given the sensing geometry and measurement model. In contrast, the EKF simulations reflect practical estimator performance, accounting for linearization errors and nonlinear dynamics.

Table 1 summarizes the comparative results. The optimized trajectory achieves a lower $\sqrt{\text{Tr}(\text{PCRLB})}$ for the target and a comparable $\sqrt{\text{Tr}(\text{PCRLB})}$ for the collaborating USV, indicating improved information geometry for the target without a significant reduction in the measurements to the supporting platform. The EKF-based Monte Carlo validation further confirms these trends by

showing a overall reduction in the standard deviation (SD), where the optimized trajectory achieves a 65.0% reduction in target standard deviation and a 12.8% improvement in USV SD. Additionally, a 10.3% reduction in total mission time relative to the racetrack baseline is achieved.

Table 1 Comparison of Optimized and Heuristic FFOV UAV Performance

Metric	Optimized FFOV UAV	Heuristic FFOV UAV
Target Data		
$\sqrt{\text{Tr}(\text{PCRLB})}$, m	0.93	2.08
Standard deviation, m	1.32	3.77
Collaborating USV Data		
$\sqrt{\text{Tr}(\text{PCRLB})}$, m	0.70	0.64
Standard deviation, m	1.64	1.88
Overall Simulation Data		
Flight time, s	47.3	52.7
Total cost	0.68	2.36

The histogram in Fig. 5 illustrates the comparative distribution of combined RMSE values obtained using the heuristic and optimized trajectories. The vertical dashed lines denote the mean RMSE across all Monte Carlo runs. The heuristic trajectory results in a highly skewed RMSE distribution with a long tail, indicating occasional severe localization failures, whereas the optimized trajectory yields better performance based on the lower mean value compared to the heuristic trajectory. Additionally, the optimized trajectory yields a significantly tighter RMSE distribution, implying better overall performance even in the worst-case scenario.

The improved $\sqrt{\text{Tr}(\text{PCRLB})}$ and SD performance of the optimized trajectory arises from how it distributes sensing opportunities over time. The racetrack trajectory focuses on the target USV during the first portion of the flight and transitions to localizing the collaborating USV in the second half. This results in highly informative and repeated observations of the target early on. However, since the estimator receives no new measurements of the target later in the mission, the final SD reflects accumulated process uncertainty. Conversely, the optimized trajectory continuously alternates between observing the target and the USV, preserving balanced observability and maintaining information flow until mission termination.

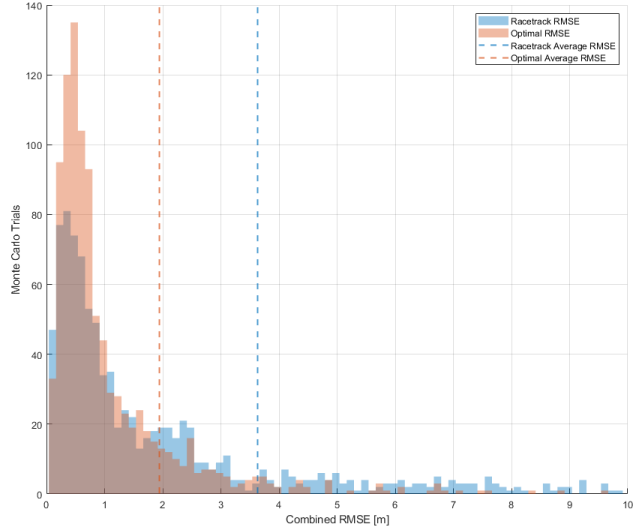


Fig. 5 Histograms for the combined RMSE for the target and collaborating USV positions. The optimized trajectory consistently reduces RMSE and eliminates large outliers while reducing mission time. The racetrack trajectory exhibits high variance and occasional severe localization failures.

These results underscore the distinction between theoretical information metrics and realized estimator behavior. The $\text{Tr}(\text{PCRLB})$ provides a necessary but not sufficient indicator of achievable performance. Estimator accuracy ultimately depends on the temporal distribution and quality of measurements. The optimized trajectory demonstrates how an information-driven design can convert theoretical observability into consistent practical performance while reducing total mission time.

The single FFOV UAV case study highlights both the benefits of trajectory optimization and the inherent limitations of FFOV platforms. Without independent sensor steering, a single UAV cannot maintain optimal observation geometry over time, making estimation performance highly sensitive to vehicle dynamics and sensing alignment. To address these limitations, the subsequent case study extends the estimation framework to compare the target localization performance achieved by a team of coordinated FFOV UAVs with that achieved by a single UAV equipped with a gimballed camera. Each FFOV UAV follows an optimized, complementary trajectory to maximize information gain. This comparison explores whether distributed coordination can compensate for individual sensor limitations and deliver comparable or superior localization performance. Additionally, the

study examines broader system-level trade-offs, including resilience, scalability, and cost, which are factors critical to future operations in contested or resource-constrained environments.

Case Study 2: UAV equipped with a gimballed camera versus Multiple Fixed Field-of-View UAVs

This case study evaluates the relative performance and system tradeoffs between a single UAV equipped with a gimballed camera and a coordinated team of FFOV UAVs for bearing-only target localization as depicted in Figs. 6 and 7, respectively. The trajectory generation process begins with a representative scenario in which one or more UAVs are deployed from a collaborating USV and tasked with localizing a stationary adversarial surface target. Each UAV operates at a constant airspeed V_A and predefined fixed altitude for airspace deconfliction.

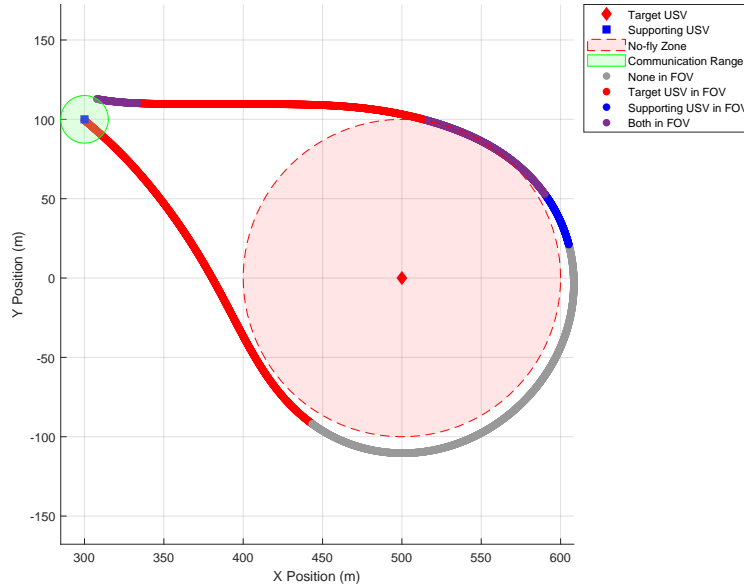


Fig. 6 Optimized UAV equipped with a gimballed camera trajectory. The UAV localizes a stationary target and a collaborating USV in minimum time while adhering to mission flight constraints. FOV segmentation along the UAV trajectory - Red: target USV in FOV. Blue: collaborating USV in FOV. Purple: both USVs visible. Gray: both USVs out of view.

In the gimballed configuration, the UAV's sensor LOS is decoupled from the UAV's body-frame kinematics. This system choice enables independent gimbal steering, maximizing visibility and information gain regardless of flight direction. As shown in Fig. 6, the UAV's trajectory is generated

using a Bernstein polynomial-based optimization method, designed to maximize target localization in minimum time while adhering to mission constraints. The FOV segmentation along the trajectory shown is color-coded to indicate periods when the target vessel (red), the collaborating USV (blue), or both (purple) are visible in the camera's LOS. Gray segments indicate periods when neither vessel is visible due to an increased bank angle as the UAV repositions.

In contrast, FFOV UAVs rely solely on airframe heading to align their sensors, necessitating coordinated group behavior to maintain near-continuous coverage. Fig. 7 shows trajectories for five FFOV UAVs optimized collectively.

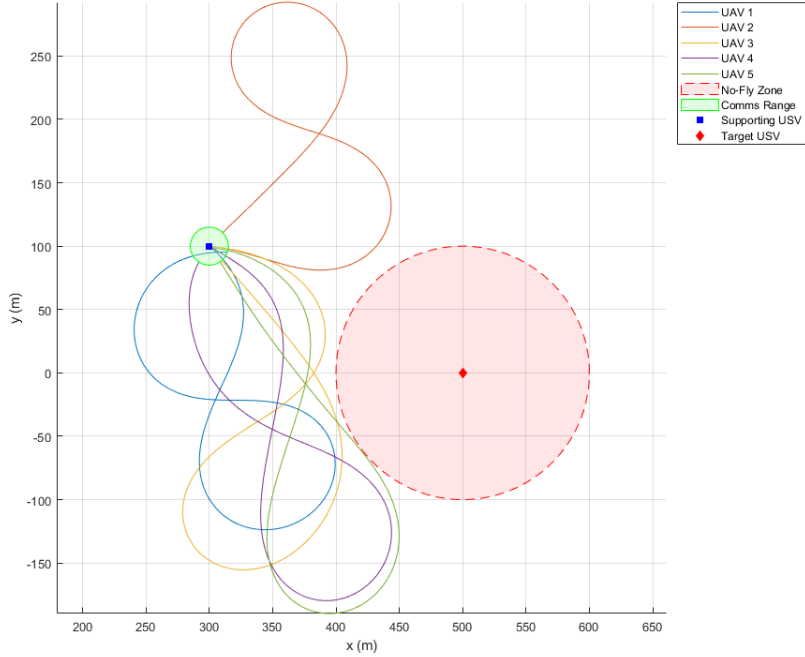


Fig. 7 Optimized trajectories for multiple FFOV UAVs. The UAVs localize a stationary target and a collaborating USV in minimum time while adhering to mission flight constraints.

Table 2 summarizes the optimization cost and corresponding lower bounds on estimation accuracy for both the target and the collaborating USV, along with the final SD achieved in simulation. Since the optimization cost, computed from Eq. 32, is a weighted sum of the target and USV terms plus the time penalty, its value is lower than either individual component. It represents a normalized, combined measure of estimation performance and mission duration.

Table 2 $\sqrt{\text{Tr}(\text{PCRLB})}$, Optimization Cost, and Final Localization Error for the Target

UAV Type	Number	$\sqrt{\text{Tr}(\text{PCRLB})}$, m		Time to Complete, s	Optimization Cost	Final Target SD, m
		Target	Collaborating USV			
Gimballed	1	1.610	1.211	32.8	0.9777	2.559
FFOV	1	7.774	2.726	38.0	1.0956	12.805
	2	4.320	1.837	43.8	1.0669	5.388
	3	3.647	1.802	43.3	1.0282	4.230
	4	2.390	1.490	33.0	0.7818	3.156
	5	1.846	1.184	31.5	0.6718	2.193

The UAV equipped with a gimballed camera achieves the smallest $\sqrt{\text{Tr}(\text{PCRLB})}$ for both the target USV. This demonstrates its estimation capability due to its ability to actively steer its camera throughout the trajectory. However, its corresponding optimization cost shows that this benefit comes with a longer mission completion time and reduced overall efficiency once the time penalty is incorporated into the cost function. The gimballed configuration therefore provides the best estimation at the expense of complexity, duration, and potential single-point vulnerability. While the UAV equipped with a gimballed camera demonstrates strong localization performance in isolation, its advantages must be weighed against its higher SWaP-C burden when assessing for scalability [33]. Gimbaled systems require more power for stabilization, introduce mechanical complexity, and constitute a single point of failure. These characteristics make such systems less attractive for large-scale or resource-constrained operations where robustness, simplicity, and cost-effectiveness are highly valued [34].

In contrast, a single FFOV UAV exhibits significantly degraded performance, with larger $\sqrt{\text{Tr}(\text{PCRLB})}$ values for both the target and collaborating USVs, a much larger target localization error, and flight duration. The higher optimization cost reflects the reduced estimation accuracy and increased flight time caused by the geometric limitations of the FFOV camera. This performance gap between the gimballed and single-FFOV camera configurations underscores the need for cooperative sensing strategies.

As the number of FFOV UAVs increases, the results show an improvement in both estimation accuracy and overall mission cost. In general, the $\sqrt{\text{Tr}(\text{PCRLB})}$ for the target and collaborating

USVs decrease with the optimization cost. The final target localization error follows a similar trend as coordination among UAVs increases. This improvement arises from the geometric diversity and increased number of measurements as each additional UAV contributes new information.

The mission completion time also decreases substantially as more FFOV UAVs are introduced. This reduction results from improved coordination and decreased need for each individual platform to reposition extensively to obtain a valid measurement. The time penalty term within the cost function amplifies the benefit of multi-UAV coordination, leading to lower total cost in both localization accuracy and time efficiency.

Table 3 provides an integrated comparison of performance and SWaP-C characteristics. Notably, teams of five or more FFOV UAVs achieve comparable or superior estimation performance to a UAV equipped with a gimballed camera, while simultaneously offering advantages in time to completion and scalability.

Table 3 Integrated Comparison of Estimation Performance and SWaP-C Metrics

UAV Type	Number	$\sqrt{\text{Tr}(\text{PCRLB})}$		Time to		
		Target	Collaborating USV	Completion	SWaP-C	Resilience
Gimballed	1	Baseline	Baseline	Baseline	High	None
FFOV	1	Poor	Poor	Poor	Low	None
	2	Poor	Near	Poor	Low	Low
	3	Near	Near	Poor	Low	Moderate
	4	Near	Near	Near	Low	High
	5	Near	Better	Better	Low	High

The data reveals that while a gimballed UAV achieves superior single-UAV estimation accuracy, multi-UAV FFOV configurations can reach comparable or better performance with reduced mission duration and cost. The five-FFOV configuration achieves similar $\sqrt{\text{Tr}(\text{PCRLB})}$ values and a smaller final target SD than the gimballed case while requiring less flight time. This suggests that multi-UAV systems, when effectively coordinated, can achieve adequate sensing at reduced costs and with enhanced resilience. Operationally, this highlights the scalability and robustness of fixed-sensor swarms where performance can be increased incrementally by adding additional low-cost UAVs rather than relying on single high-capability platforms. The FFOV system therefore offers superior

resilience and scalability. Its reduced SWaP-C burden enables deployment in larger numbers, making it a compelling alternative for cost-sensitive or contested environments where attrition, endurance, or resource constraints are operational concerns.

IV. Conclusion

This paper investigated how trajectory optimization and sensor architecture affect bearing-only target localization using UAVs operating in GPS-denied environments. An information-theoretic optimization framework was developed to generate dynamically feasible trajectories using Bernstein polynomial parameterization, while a FKF was used to fuse measurements and assess estimator performance.

The results showed that estimation-aware trajectory optimization substantially improves localization accuracy compared with heuristic flight paths, and that estimator performance closely approaches the theoretical PCRLB limit. Coordinated teams of FFOV UAVs were found to match or surpass the localization accuracy of a single gimballed platform while requiring less mission time and lower SWaP-C. These findings confirm that coordinated FFOV systems offer a practical, resilient alternative to mechanically complex gimballed UAV systems in contested environments.

The Bernstein polynomial parameterization played a critical role in enabling smooth, dynamically feasible trajectories that satisfied constraints such as NFZ avoidance, communication bounds, and platform limitations, while accounting for out-of-frame events. The study showed that trajectory optimization is not merely a control problem but a systems-level design tool that links estimation performance with practical mission considerations. These insights have direct implications for both tactical and commercial UAV operations. For military operations, FFOV UAV teams can enable targeting and over-the-horizon surveillance under SWaP-C and stealth constraints. In commercial applications, multi-agent FFOV systems may offer scalable, cost-effective solutions for inspection, mapping, and search-and-rescue missions.

This work demonstrates that estimation-aware trajectory design enables scalable, resilient, and cost-effective UAV system designs for use in GPS-denied and contested environments.

Appendix

Table 4 Optimization weighting parameters for Case Studies 1 and 2

Parameter	Symbol	Value	
		Case Study 1	Case Study 2
Target weighting factor	w_1	0.5	0.9
Collaborating USV weighting factor	w_2	0.5	0.1
Time penalty weighting factor	w_3	0.5	0.4

Table 5 Common simulation parameters for all UAV configurations

Parameter	Symbol	Value
No-fly zone radius	r_{NFZ}	100 m
Communication range	r_{com}	15 m
Initial time estimate	t_f	30 s
UAV speed	V_A	25 m/s
Maximum roll angle	ϕ^{\max}	$\pi/4$ rad
Camera sample rate	f	1 Hz
Measurement noise variance	σ^2	7.5×10^{-6} rad
Process noise variance	σ_w^2	0.49
FFOV camera boresight angle	–	$\pi/4$ rad
Camera resolution (pixels)	–	2592×1944

Table 6 Simulation parameters for the gimballed UAV configuration

Parameter	Symbol	Value
Maximum azimuth angle	ψ_g^{\max}	$\pi/2$ rad
Minimum azimuth angle	ψ_g^{\min}	$-\pi/2$ rad
Maximum elevation angle	θ_g^{\max}	$\pi/2$ rad
Minimum elevation angle	θ_g^{\min}	0 rad
Maximum azimuth slew rate	$u_{\psi_g}^{\max}$	5.24 rad/s
Minimum azimuth slew rate	$u_{\psi_g}^{\min}$	-5.24 rad/s
Maximum elevation slew rate	$u_{\theta_g}^{\max}$	5.24 rad/s
Minimum elevation slew rate	$u_{\theta_g}^{\min}$	-5.24 rad/s

References

[1] Telli, K., Kraa, O., Himeur, Y., Ouamane, A., Boumehraz, M., Atalla, S., and Mansoor, W., “A Comprehensive Review of Recent Research Trends on Unmanned Aerial Vehicles (UAVs),” *Systems*, Vol. 11, No. 88, 2023, p. 400. <https://doi.org/10.3390/systems11080400>.

[2] Krystosik-Gromadzińska, A., “The use of drones in the maritime sector – areas and benefits,” *Zeszyty Naukowe Akademii Morskiej w Szczecinie*, Vol. nr 67 (139), 2021. <https://doi.org/10.17402/473>.

[3] Chung, S.-J., Paranjape, A. A., Dames, P., Shen, S., and Kumar, V., “A Survey on Aerial Swarm Robotics,” *IEEE Transactions on Robotics*, Vol. 34, No. 4, 2018, p. 837–855. <https://doi.org/10.1109/TRO.2018.2857475>.

[4] Peck, M., “The reign of the Reaper drone may be coming to an end,” , May 2025. URL <https://www.businessinsider.com/reign-of-drones-like-us-reaper-may-be-ending-2025-5>.

[5] Hambling, D., “Hidden Killers: Inside Ukraine’s Combat Drone Statistics,” , Apr. 2025. URL <https://www.forbes.com/sites/davidhambling/2025/04/16/hidden-killers-inside-ukraines--combat-drone-statistics/>.

[6] Hammel, S. E., Liu, P. T., Hilliard, E. J., and Gong, K. F., “Optimal observer motion for localization with bearing measurements,” *Computers & Mathematics with Applications*, Vol. 18, No. 1, 1989, pp. 171–180. [https://doi.org/10.1016/0898-1221\(89\)90134-X](https://doi.org/10.1016/0898-1221(89)90134-X).

[7] Oshman, Y., and Davidson, P., “Optimization of observer trajectories for bearings-only target localization,” *IEEE Transactions on Aerospace and Electronic Systems*, Vol. 35, No. 3, 1999, pp. 892–902. <https://doi.org/10.1109/7.784059>.

[8] Ponda, S., Kolacinski, R., and Frazzoli, E., “Trajectory Optimization for Target Localization Using Small Unmanned Aerial Vehicles,” *AIAA Guidance, Navigation, and Control Conference*, American Institute of Aeronautics and Astronautics, 2009, pp. 1–25. <https://doi.org/https://doi.org/10.2514/6.2009-6015>.

[9] Vander Hook, J., Tokekar, P., and Isler, V., “Algorithms for Cooperative Active Localization of Static Targets With Mobile Bearing Sensors Under Communication Constraints,” *IEEE Transactions on Robotics*, Vol. 31, No. 4, 2015, pp. 864–876. <https://doi.org/10.1109/TRO.2015.2432612>.

[10] Ristic, B., Arulampalam, S., and Gordon, N., *Beyond the Kalman Filter: Particle Filters for Tracking Applications*, Artech House, 2003, Chaps. 4,6, pp. 67–80, 103–138.

[11] Yokoyama, N., and Ochi, Y., “Path Planning Algorithms for Skid-to-Turn Unmanned Aerial Vehicles,” *Journal of Guidance, Control, and Dynamics*, Vol. 32, No. 5, 2009, p. 1531–1543. <https://doi.org/10.2514/1.41822>.

[12] Chai, R., Savvaris, A., Tsourdos, A., Xia, Y., and Chai, S., “Solving Multiobjective Constrained Trajectory Optimization Problem by an Extended Evolutionary Algorithm,” *IEEE Transactions on Cybernetics*, Vol. 50, No. 4, 2020, p. 1630–1643. <https://doi.org/10.1109/TCYB.2018.2881190>.

[13] Van Trees, H. L., Bell, K. L., and Tian, Z., *Detection, Estimation, and Modulation Theory, Part I: Detection, Estimation, and Filtering Theory*, 2nd ed., Wiley, 2013, Chap. 2, pp. 66–68.

[14] Passerieux, J., and Van Cappel, D., “Optimal observer maneuver for bearings-only tracking,” *IEEE Transactions on Aerospace and Electronic Systems*, Vol. 34, No. 3, 1998, pp. 777–788. <https://doi.org/10.1109/7.705885>.

[15] Ousingsawat, J., and Campbell, M. E., “Optimal Cooperative Reconnaissance Using Multiple Vehicles,” *Journal of Guidance, Control, and Dynamics*, Vol. 30, No. 1, 2007, pp. 122–132. <https://doi.org/10.2514/1.19147>.

[16] Lee, W., Bang, H., and Leeghim, H., “Cooperative localization between small UAVs using a combination of heterogeneous sensors,” *Aerospace Science and Technology*, Vol. 27, No. 1, 2013, pp. 105–111. <https://doi.org/10.1016/j.ast.2012.07.002>.

[17] Robinson, D. R., Mar, R. T., Estabridis, K., and Hewer, G., “An Efficient Algorithm for Optimal Trajectory Generation for Heterogeneous Multi-Agent Systems in Non-Convex Environments,” *IEEE Robotics and Automation Letters*, Vol. 3, No. 2, 2018, p. 1215–1222. <https://doi.org/10.1109/LRA.2018.2794582>.

[18] Cichella, V., Kaminer, I., Walton, C., and Hovakimyan, N., “Optimal Motion Planning for Differentially Flat Systems Using Bernstein Approximation,” *IEEE Control Systems Letters*, Vol. 2, No. 1, 2018, pp. 181–186. <https://doi.org/10.1109/LCSYS.2017.2778313>.

[19] Cichella, V., Kaminer, I., Walton, C., Hovakimyan, N., and Pascoal, A. M., “Optimal Multivehicle Motion Planning Using Bernstein Approximants,” *IEEE Transactions on Automatic Control*, Vol. 66, No. 4, 2021, pp. 1453–1467. <https://doi.org/10.1109/TAC.2020.2999329>.

[20] Farouki, R. T., “The Bernstein polynomial basis: A centennial retrospective,” *Computer Aided Geometric Design*, Vol. 29, No. 6, 2012, pp. 379–419. <https://doi.org/https://doi.org/10.1016/j.cagd.2012.03.001>.

[21] Mudrik, L., Sciacchitano, A., Kragelund, S., Kang, J., and Kaminer, I., “Optimization of Observer Trajectory for Coordinated Bearing-Only Localization in Constrained Three-Dimensional Scenarios,” *AIAA SciTech Forum*, American Institute of Aeronautics and Astronautics, Orlando, FL, 2025, pp. 1–19. <https://doi.org/10.2514/6.2025-2604>.

[22] Ning, Z., Zhang, Y., Li, J., Chen, Z., and Zhao, S., “A bearing-angle approach for unknown target motion analysis based on visual measurements,” *The International Journal of Robotics Research*, Vol. 43, No. 8, 2024, p. 1228–1249. <https://doi.org/10.1177/02783649241229172>.

[23] Kragelund, S., Walton, C., Kaminer, I., and Dobrokhodov, V., “Generalized Optimal Control for Autonomous Mine Countermeasures Missions,” *IEEE Journal of Oceanic Engineering*, Vol. 46, No. 2, 2021, p. 466–496. <https://doi.org/10.1109/JOE.2020.2998930>.

[24] Andersson, J. A. E., Gillis, J., Horn, G., Rawlings, J. B., and Diehl, M., “CasADi: a software framework for nonlinear optimization and optimal control,” *Mathematical Programming Computation*, Vol. 11, No. 1, 2019, p. 1–36. <https://doi.org/10.1007/s12532-018-0139-4>.

[25] Tichavsky, P., Muravchik, C., and Nehorai, A., “Posterior Cramer-Rao bounds for discrete-time nonlinear filtering,” *IEEE Trans. Signal Process.*, Vol. 46, No. 5, 1998, pp. 1386–1396. <https://doi.org/10.1109/78.668800>.

[26] Kielas-Jensen, C., Cichella, V., Casbeer, D., Manyam, S. G., and Weintraub, I., “Persistent Monitoring by Multiple Unmanned Aerial Vehicles Using Bernstein Polynomials,” *J Optim Theory Appl*, Vol. 191, No. 2, 2021, pp. 899–916. <https://doi.org/10.1007/s10957-021-01921-z>.

[27] Kielas-Jensen, C., Cichella, V., Berry, T., Kaminer, I., Walton, C., and Pascoal, A., “Bernstein Polynomial-Based Method for Solving Optimal Trajectory Generation Problems,” *Sensors*, Vol. 22, No. 5, 2022, p. 1869. <https://doi.org/10.3390/s22051869>.

[28] Cichella, V., Kaminer, I., Walton, C., Hovakimyan, N., and Pascoal, A., “Consistency of Approximation

of Bernstein Polynomial-Based Direct Methods for Optimal Control,” *Machines*, Vol. 10, No. 12, 2022, p. 1132. <https://doi.org/10.3390/machines10121132>.

[29] Tabasso, C., and Cichella, V., “On-line Motion Planning Using Bernstein Polynomials for Enhanced Target Localization in Autonomous Vehicles,” , Apr. 2024. <https://doi.org/10.48550/arXiv.2210.03187>.

[30] Carlson, N., “Federated square root filter for decentralized parallel processors,” *IEEE Transactions on Aerospace and Electronic Systems*, Vol. 26, No. 3, 1990, pp. 517–525. <https://doi.org/10.1109/7.106130>.

[31] Carlson, N. A., and Berarducci, M. P., “Federated Kalman Filter Simulation Results,” *NAVIGATION*, Vol. 41, No. 3, 1994, pp. 297–322. <https://doi.org/10.1002/j.2161-4296.1994.tb01882.x>.

[32] Kim, J., Jee, G.-I., and Lee, J. G., “A Federated Kalman Filter Design Using a Gain Fusion Algorithm,” *IFAC Proceedings Volumes*, Vol. 31, No. 21, 1998, p. 385–391. [https://doi.org/10.1016/S1474-6670\(17\)41107-4](https://doi.org/10.1016/S1474-6670(17)41107-4).

[33] Korobov, N., Shipitko, O., Konovalenko, I., Grigoryev, A., and Chukalina, M., “SWaP-C Based Comparison of Onboard Computers for Unmanned Vehicles,” *Proceedings of 14th International Conference on Electromechanics and Robotics “Zavalishin’s Readings”*, edited by A. Ronzhin and V. Shishlakov, Springer, Singapore, 2020, p. 573–583. https://doi.org/10.1007/978-981-13-9267-2_47.

[34] Petritoli, E., Lecce, F., and Ciani, L., “Reliability and Maintenance Analysis of Unmanned Aerial Vehicles,” *Sensors (Basel, Switzerland)*, Vol. 18, No. 9, 2018, p. 3171. <https://doi.org/10.3390/s18093171>.